Chapter 6

Physics performance

6.1 Principle of proton reconstruction

Protons emerging from elastic and diffractive scattering at LHC are emitted at very small angles (10 to 150 μrad) and undergo no or small ($10^{-7} \div 0.1$) fractional momentum loss ($\xi = |\Delta p|/p$), respectively. Hence they are very close to the beam and can only be detected in the RP detectors downstream symmetrically on either side of the interaction point (IP) if their displacement at the detector location is large enough.

The transverse displacement $(x(s), y(s))$ of an elastically or diffractively scattered proton at a distance s from the IP is related to its origin $(x^*, y^*, 0)$, scattering angles $\Theta^*_{x,y}$ and ξ value at the IP via the optical functions L, v, D as described in chapter 3. The optical functions (L, v, D) determining the explicit path of the particle through the magnetic elements, depend mainly on the position along the beam line (i.e. on all the magnetic elements traversed before reaching that position and their settings which is optics dependent) but also on the particle parameters at the IP (3.2).

The proton tracking through the accelerator lattice is based on the parametrization of the optical functions (extracted for each configuration from the program MAD-X [47]); their slight dependency on the kinematic variables, $\Theta^*_{x,y}$ and ξ, is also taken into account [48].

The transverse vertex position and the scattering angle at the IP are smeared assuming Gaussian distributions with widths given by the transverse beam size and the beam divergence, both determined by β^* and by the (normalised) emittance ε_n. Table 6.1 summarises the beam parameters at the IP for the different optics settings. In addition an energy spread of 10^{-4} is always assumed. The minimum distance of a RP station to the beam on one hand and constraints imposed by the beam pipe or beam screen size [49] on the other hand will determine the proton acceptance of a RP station. The minimum distance of a RP to the beam is proportional to the beam size $((10-15) \times \sigma_{x(y)}(s))$.

6.1.1 Acceptance

The acceptance of the RP system for elastically or diffractively scattered protons depends on the optics configuration. The complementarity of the acceptance of different optics configurations is shown in figure 6.1. As discussed in chapter 3, the TOTEM-specific optics with $\beta^* = 1540$ m was

Table 6.1: Parameters of the different optics settings at nominal emittance ε_n=3.75 μm·rad ($\varepsilon_n = 1\,\mu\text{m}\cdot\text{rad}$ for β^*=1540 m).

β^* [m]	crossing angle [μrad]	IP offset in x [μm]	IP beam size [μm]	IP beam divergence [μrad]
1540	0	0	450	0.3
90	0	0	213	2.3
2	92	322	32	16

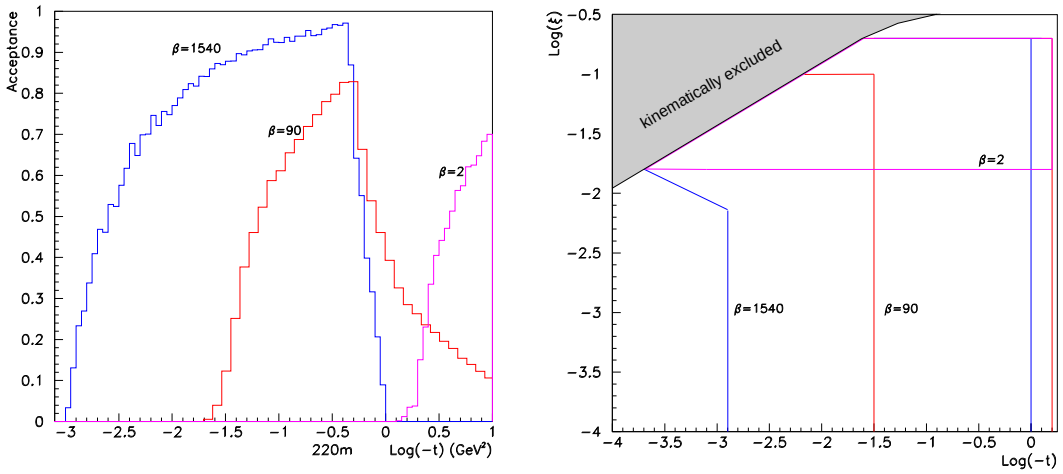

Figure 6.1: Left: acceptance in $\log_{10}|t|$ for elastically scattered protons at the Roman Pot station at 220 m for different optics settings. Right: acceptance in $\log_{10}|t|$ and $\log_{10}\xi$ for diffractively scattered protons at the same RP station for different optics settings. The contour lines represent the 10% level.

particularly optimised for accepting protons down to very low $|t|$-values and — in the diffractive case — with all kinematically allowed values of ξ (blue graphs in figure 6.1, left and right, respectively). With the $\beta^* = 90\,\text{m}$ optics, diffractive scattered protons are still accepted independently from their ξ-value, but the t-acceptance is reduced compared to $\beta^* = 1540\,\text{m}$ optics (red graphs in figure 6.1, right and left, respectively). With high luminosity optics ($\beta^* = 0.5\,\text{m} \div 2\,\text{m}$) on the other hand, the diffractive protons are within the acceptance of the RP detectors because of their ξ value almost independently of their t value (magenta graph in figure 6.1, right). In addition, elastically scattered protons can be detected at very large t (see magenta graph in figure 6.1, left).

The complementarity of the different optics configurations in the measurement of elastic and central diffraction cross-section is shown in figure 6.2. In elastic events (figure 6.2, left), the full t-range from 0.002 up to $10\,\text{GeV}^2$ will be covered by combining data from runs at several optics configurations. With typical running times of 10^5 s (i.e. a bit more than a day), enough statistics can be accumulated for each interval (see table 6.2). The statistics is also sufficient for the physics alignment of the RP detectors. The overlapping regions between the acceptances of the different optics configurations will allow for cross-checks of the measurements.

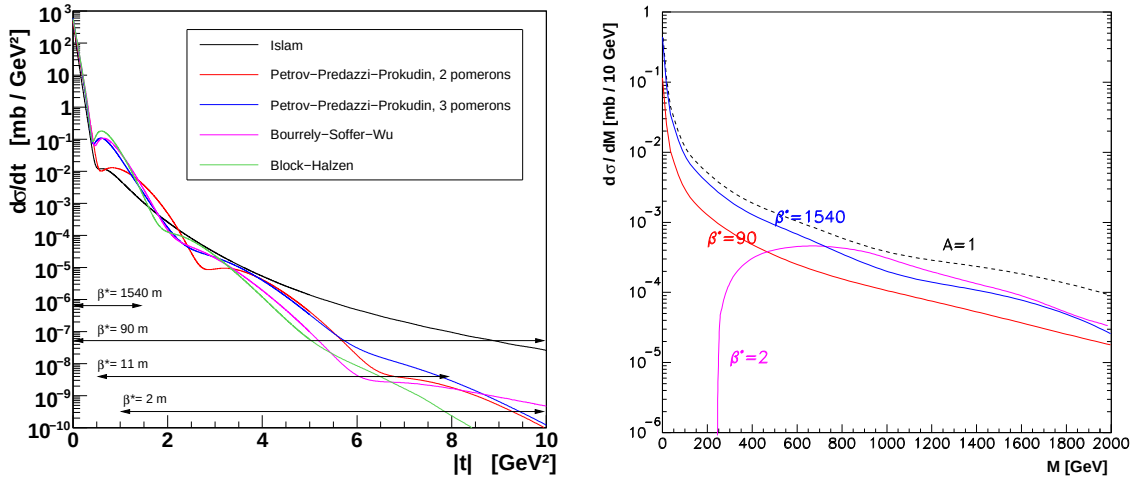

Figure 6.2: Left: differential cross-section of elastic scattering at $\sqrt{s}$ = 14 TeV as predicted by various models together with the t-acceptance ranges of different optics settings. Right: predicted differential cross-section of central diffraction at $\sqrt{s} = 14$ TeV with (solid) and without (dashed) taking the proton acceptance into account for different optics settings.

Figure 6.2 (right) shows the predicted central diffractive mass distribution together with the acceptance corrected distributions for three different optics settings. With the high and intermediate β^* optics, all diffractive masses, down to the lowest values are observable. For low-β^* optics on the other hand, the acceptance starts at around 250 GeV but has the advantage of better statistics for high masses due to the higher luminosity. By combining data from runs at low-β^* optics with data from high or intermediate optics runs, the differential cross-section as function of the central diffractive mass can be measured with good precision over the full mass range.

6.1.2 Reconstruction of diffractive proton kinematics

The reconstruction procedure for diffractively scattered protons aims at a determination of the kinematics parameters $\Theta_{x,y}$ and ξ of the proton. For elastic scattering, i.e. when $\xi = 0$, the reconstruction is simpler and will be discussed more in detail in section 6.1.3. In the following, the reconstruction procedure and its performance for diffractive protons with the $\beta^* = 90$ m optics will be discussed in detail. The reconstruction performance for other optics will only be briefly summarised.

6.1.2.1 Diffractive proton reconstruction with the $\beta^* = 90$ m optics

The transverse coordinates of the proton at the IP (x^*, y^*, see eq. (3.2)) are considered as additional free variables since their uncertainty contribute significantly to the reconstruction uncertainty, especially for the high β^* optics characterised by large beam sizes at the IP. To reconstruct the full set of kinematic variables, $(\Theta_x, \Theta_y, x^*, y^*, \xi)$, the proton transport equations (3.2) are inverted by χ^2 minimisation procedure [48, 50].

Table 6.2: Expected number of collected elastic scattering events in different t-intervals for the BSW model in runs lasting 10^5 s (i.e. slightly more than a day) with different optics settings.

$\lvert t\rvert$-range [GeV^2]	β^* [m]	typical $\mathscr{L}$ [cm^{-2}s^{-1}]	Events / 10^5 s	
$0.0012 \div 0.03$	1540	10^{28}	1×10^7	or $20 \times 10^3/10^{-3}\,\text{GeV}^2$
$0.03 \div 0.5$	1540	10^{28}	1.4×10^7	or $28 \times 10^3/10^{-3}\,\text{GeV}^2$
	90	10^{30}	7.5×10^8	or $1.5 \times 10^6/10^{-3}\,\text{GeV}^2$
$0.5 \div 2$	90	10^{30}	5×10^5	or $300/10^{-3}\,\text{GeV}^2$
	11	10^{32}	8×10^7	or $48 \times 10^3/10^{-3}\,\text{GeV}^2$
	2	10^{33}	1×10^7	or $6 \times 10^3/10^{-3}\,\text{GeV}^2$
$2 \div 3$	90	10^{30}	1.4×10^3	or $1.4/10^{-3}\,\text{GeV}^2$
	11	10^{32}	1.4×10^5	or $140/10^{-3}\,\text{GeV}^2$
	2	10^{33}	1.1×10^6	or $1100/10^{-3}\,\text{GeV}^2$
$3 \div 6$	90	10^{30}	170	or $56/\text{GeV}^2$
	11	10^{32}	17×10^3	or $5600/\text{GeV}^2$
	2	10^{33}	430×10^3	or $143 \times 10^3/\text{GeV}^2$
$6 \div 10$	2	10^{33}	500	or $125/\text{GeV}^2$

The resolution in ξ of diffractively scattered protons using only information from the RP station at 220 m is shown in figure 6.3 (left). The ξ-resolution is about 6×10^{-3}, except for large $|t|$ ($> 1\,\text{GeV}^2$), where it worsens, and large ξ (> 0.01) where it improves. If the scattering vertex can be determined to a precision of $30\,\mu$m with the central CMS detector during common data taking, the ξ-resolution improves to about 1.6×10^{-3} [2]. The corresponding t-resolution is almost independent of ξ and ranges from $3 \times 10^{-3}\,\text{GeV}^2$ at $t = -1 \times 10^{-2}\,\text{GeV}^2$ to $1\,\text{GeV}^2$ at $t = -10\,\text{GeV}^2$ [48]. The ξ and the t determination will e.g. be used for measuring the diffractive mass ($\approx \sqrt{s\xi}$) and t distribution for single diffractive events.

Further studies showed that including the information from a RP station at 147 m improves the performance only slightly and only for large $|t|$ due to large contributions to the uncertainty from multiple scattering in the detectors and window material of the RP station at 147 m.

In the case of central diffraction, the two protons originate from a common scattering vertex position which slightly improves the reconstruction resolution. The resolution in the diffractive mass, reconstructed purely from the proton information according to

$$M^2 = \xi_1\,\xi_2\,s\,, \tag{6.1}$$

where $\sqrt{s} = 14\,\text{TeV}$, is shown in figure 6.3 (right). The mass resolution ranges from 40 GeV for symmetric events, i.e. those with $\xi_1 \approx \xi_2$, to 180 GeV for the very asymmetric events, where one of the ξ values is three orders of magnitude larger than the ξ value of the other. If the scattering vertex can be determined to a precision of $30\,\mu$m with the central CMS detector during common running, the mass resolution improves by approximatively a factor three [2].

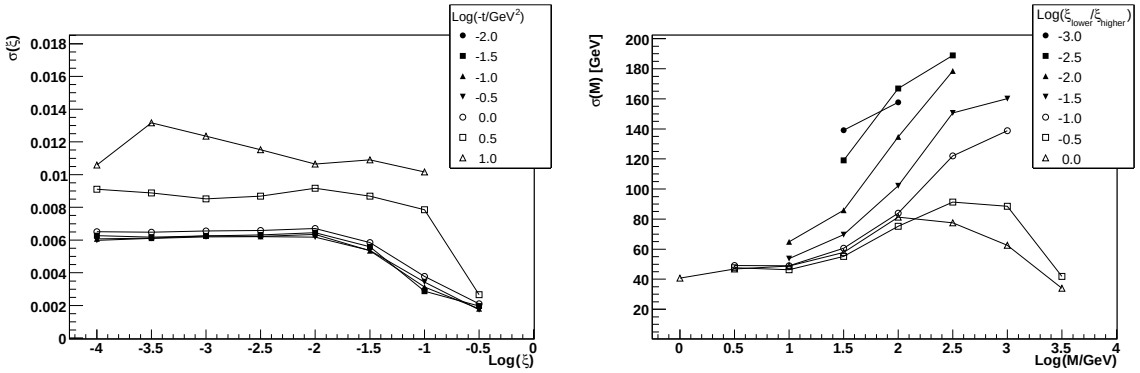

Figure 6.3: Left: resolution for the ξ reconstruction of a single diffractive proton based only on the information from the RP station at 220 m at $\beta^* = 90$ m optics. The different markers corresponds to the resolution at different $\log_{10}(-t)$ values. Right: resolution on the reconstruction of the central mass based on the measurement of the two scattered protons in central diffractive events for $\beta^* = 90$ m optics. Both protons are reconstructed with the RP stations at 220 m. The different markers corresponds to different values of the $\xi_{\text{lower}}/\xi_{\text{higher}}$ ratio, where ξ_{lower} (ξ_{higher}) is the ξ-value of the proton that lost less (more) momentum.

6.1.2.2 Diffractive proton reconstruction performance with other optics

At low β optics only protons with a ξ above 0.02 are detected with a RP station at 220 m. The ξ resolution ranges from 1×10^{-3} at $\xi = 0.02$ to 2×10^{-3} at $\xi = 0.2$ with only a small t dependence. If both protons are detected at the 220 m location, the accepted mass of the central system in central diffractive events is larger than 250 GeV and the mass resolution ranges from 5 GeV for a central mass of 250 GeV to 20 GeV for a central mass of 2.5 TeV. All accepted events are more or less symmetric, i.e. $\xi_1 \approx \xi_2$, due to the limited ξ acceptance. For further details see ref. [2].

With $\beta^* = 1540$m optics, protons are detected independently of their ξ but the large beam size at the IP and large L_x value complicates the disentangling of the x^*, Θ_x^* and ξ contributions to the horizontal displacement of the proton at the RP station. To constrain the parameters, information from both the RP station at 147 and 220 m are used for the reconstruction. The ξ resolution of this method ranges between 5 to 10×10^{-3} with dependencies on the azimuthal angle and the size of t. The accepted mass of the central system in central diffractive events spans the whole mass range for this optics. The resolution on the central mass ranges in the best case, for symmetric events, from 50 GeV for a mass of 50 GeV, to 80 GeV for a mass of 2 TeV. A more detailed description of the reconstruction method and the performance can be found in ref. [2, 50].

6.1.3 Reconstruction of elastic protons

Here the algorithm for the reconstruction of elastic events is briefly described. The detailed description can be found in ref. [51]. The algorithm consists in the following three steps:

- Selection of elastic proton candidates: RP detector hits belonging to the particle tracks of elastic protons (in both arms) are selected.

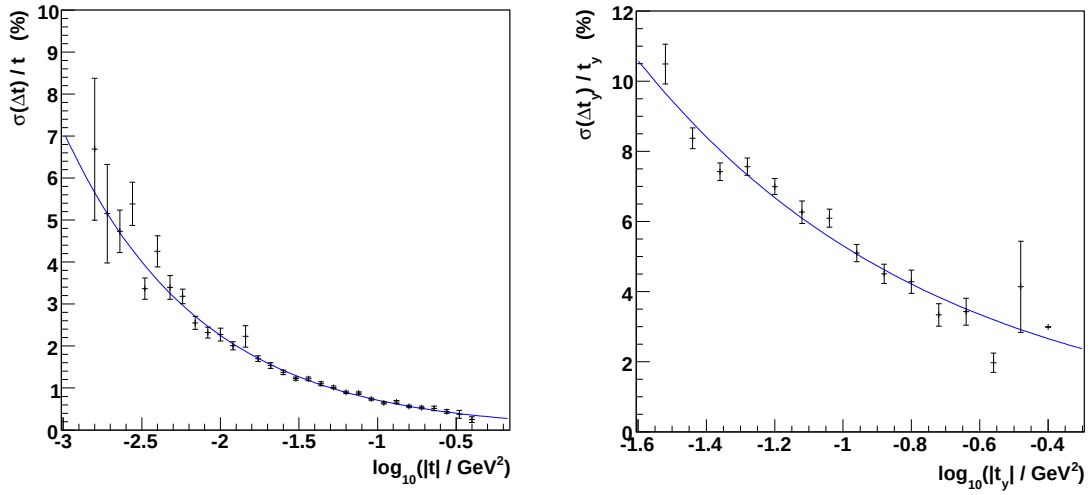

Figure 6.4: Relative resolution on t (left) and t_y (right) from the elastic event reconstruction based on the RP stations at 220 m with $\beta^* = 1540$ m and $\beta^* = 90$ m optics respectively. The solid line in the left (right) plot shows the expected $1/\sqrt{|t|}$ ($1/\sqrt{|t_y|}$) dependence.

- Fitting of the proton kinematics. Three fits made: one for the right arm fit, one for the left arm and a global one. The fits are made using a linear model approach based on the proton transport equations (3.2).

- Final selection. Fits for the left and right arm are compared. The differences in the reconstructed scattering angles Θ_x^*, Θ_y^* and vertex positions x^*, y^* are required to be within the expected uncertainties. For events passing all selections, the global fit is taken as the result.

With $\beta^* = 1540$ m, both effective lengths, L_x and L_y, are large and both magnifications, v_x and v_y, small at the RP station of 220 m enabling the measurement of both projections of the scattering angle and hence the unambiguous reconstruction of $t = t_x + t_y$, where $t_x \equiv t\cos^2\varphi \approx (p\Theta_x^*)^2$ and $t_y \equiv t\sin^2\varphi \approx (p\Theta_y^*)^2$. The relative precision of the t measurement with $\beta^* = 1540$ m optics is shown in figure 6.4 (left) and follows the expected $1/\sqrt{|t|}$ dependence.

With $\beta^* = 90$ m on the other hand, $L_x(220\,\text{m})$ at the RP station at 220 m is zero. Hence in this station only the y-component of the scattering angle is measured and only the t_y component reconstructed. The relative precision of the t measurement with $\beta^* = 90$ m optics is shown in figure 6.4 (right) and follows the expected $1/\sqrt{|t_y|}$ dependence.

6.2 Measurement of inelastic events

6.2.1 Track and vertex reconstruction

T1 and T2 have been designed with the goal of detecting primary particles to reconstruct the primary vertex with a precision sufficient to discriminate beam-beam events from the background (mainly beam-gas events and halo muons). Due to the very low angle with respect to the beam of

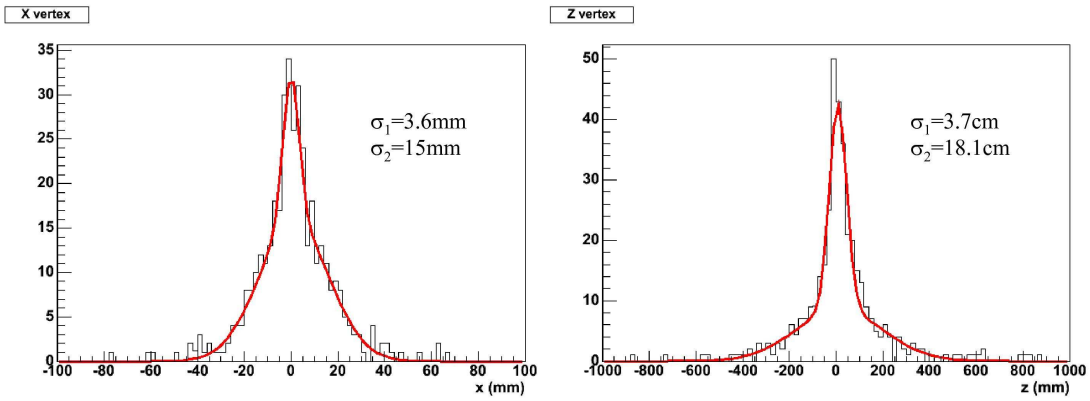

Figure 6.5: Simulated vertex reconstruction capability for T1 in the transverse plane (left) and longitudinally (right).

the charged tracks detected in the telescopes, a good spatial resolution is needed: T1 provides an average single hit resolution of ~ 0.8 mm while T2 provides a radial resolution of $\sim$100 μm. Simulations show that in presence of the CMS magnetic field, the primary vertex can be reconstructed with a precision of $\sim$1.5 cm in the radial direction and $\sim$20 cm in the beam direction (figure 6.5). Resolutions one order of magnitude better can be achieved running with the CMS magnetic field switched off.

The main background in the cross-section measurement comes from beam-gas events, which can be largely rejected with the obtained accuracy on the primary vertex reconstruction. Simulation studies show that only $\sim$3% of the beam-gas events are misidentified as beam-beam, corresponding to a rate below 1 Hz ([1], p. 191) for a running scenario with $k = 156$ bunches à 1.15×10^{11} protons.

6.2.2 Trigger acceptance

The L1 trigger in T1 is generated combining the digital signals coming from different groups of anode wires, to maximise the signal generation speed, while in T2 the L1 trigger is generated combining the signals coming from arrays of pads from different planes. An efficient trigger is a key point in avoiding biases in the measurement of the total or diffractive cross-section. With a double-arm trigger more than 99% of non-diffractive events can be detected, while with a single arm trigger one can detect the events escaping the double-arm trigger and most of the diffractive interactions that have all visible tracks in only one arm.

Dedicated studies show that single and double diffractive events are responsible for the major loss in the inelastic rate; with a single-arm trigger, a fraction of these events, corresponding to $\sim$2.8 mb, escapes detection. The lost events are mainly those with a very low mass (below $\sim$10 GeV/c^2), since all their particles are produced at pseudo-rapidities beyond the T2 acceptance and escape therefore the detection. To obtain the total inelastic rate, the fraction of events lost be-

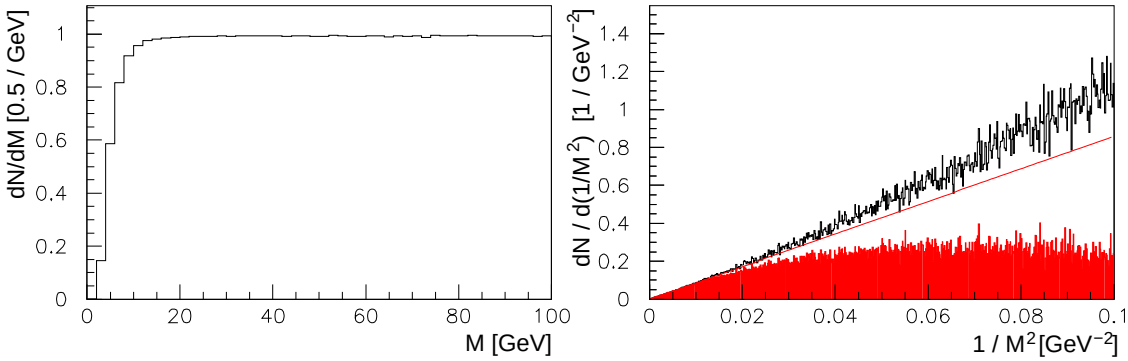

Figure 6.6: Left: ratio of detected Single Diffractive events as a function of the diffractive mass, M. Right: simulation (unshaded) and acceptance corrected (shaded) Single Diffractive distribution as function of $1/M^2$. The line shows a linear fit based on the acceptance corrected events in the mass region above $10\,\mathrm{GeV}/c^2$.

cause of the incomplete angular coverage can be estimated by extrapolation. In the case of single diffraction, the reconstructed $1/M^2$ distribution has been linearly fitted for $M > 10\,\mathrm{GeV}/c^2$, and the extrapolation to low masses has then be compared with simulation. For Single Diffraction, the extrapolated number of events differs from the simulation expectations by 4%, corresponding to a 0.6 mb uncertainty on the total cross-section (figure 6.6). The same estimation for the Double Diffraction and Double Pomeron Exchange gives a 0.1 mb and 0.2 mb uncertainty, respectively.

In the study of diffraction, the telescopes can be used to trigger and/or measure rapidity gaps. Best result are expected in combined running of the TOTEM and CMS detectors; nevertheless studies show that using only T1 and T2 telescopes, the rapidity gaps in DPE events can be measured with a precision $\lesssim 1$ unit of rapidity. Moreover, the comparison of results from SD and DPE events open the possibility of estimate the rapidity gap survival probability at LHC energies.

6.3 Total cross-section measurement

The total pp cross-section, σ_{tot}, will be measured first in runs with the $\beta^* = 90\,\mathrm{m}$ optics and later — with better precision — with the $\beta^* = 1540\,\mathrm{m}$ optics (chapter 3). The method based on the Optical Theorem and the quantities to be measured have been explained in section 2.1. The total uncertainty of σ_{tot} has the following contributions.

6.3.1 Inelastic rate

The uncertainty on the inelastic rate is dominated by the inelastic trigger losses $\delta(N_{\mathrm{inel}})/N_{\mathrm{inel}} \approx 1\%$ as discussed in section 6.2.2. The second component — trigger contamination by beam-gas background — is much smaller. This estimate is almost independent from the beam optics, exceptions being SD and DPE where for some trigger strategies leading protons are parts of the signature.

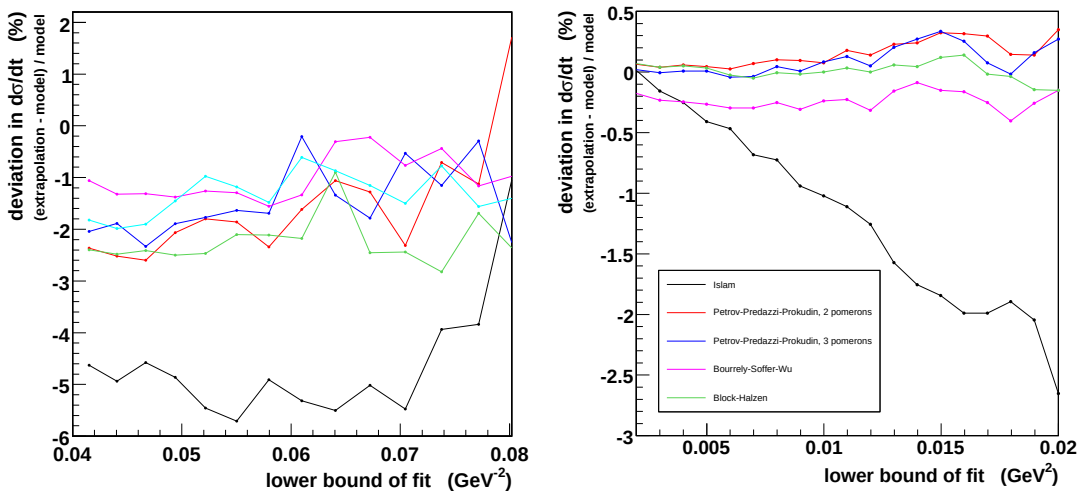

Figure 6.7: Relative deviation of the extrapolation results based on a simulation (not including an error on L_x). Left: $\beta^* = 90\,\text{m}$, right: $\beta^* = 1540\,\text{m}$. The t_y- and t-distributions were fitted from the indicated lower bound (abscissa) to $0.25\,\text{GeV}^2$ and $0.04\,\text{GeV}^2$, respectively. The different solid lines corresponds to different models.

6.3.2 Elastic rate and extrapolation of the cross-section to t = 0

The determination of σ_{tot} requires two aspects of elastic scattering to be measured: the total elastic rate and the extrapolation of the differential cross-section $d\sigma/dt$ to the Optical Point $t = 0$. Obviously, to be complete, the measured elastic rate has to be complemented by the extrapolated part, so that this extrapolation enters twice in the procedure.

At $\beta^* = 90$ m, protons with $|t| > 0.03\,\text{GeV}^2$ are observed in the RP detector at 220 m (chapter 3). The starting point of the acceptance lies well above the region where the delicate effects from the interference between nuclear and Coulomb scattering play a role. Hence for the early running optics no such perturbation needs to be included in the extrapolation procedure, in contrast to the extrapolation at the $\beta^* = 1540\,\text{m}$ optics with $|t|_{\text{min}} = 10^{-3}\,\text{GeV}^2$.

As shown in section 2.2 (figure 2.4), most theoretical models [7] predict an almost exponential behaviour of the cross-section up to $|t| \approx 0.25$ GeV^2. For all the models considered — except for the one by Islam et al. — the deviations are small. In the t-range mentioned, the slope $B(t)$ (figure 2.4, right) can be well described by a parabola, which is therefore used for the fitting function and the extrapolation. Since this quadratic behaviour of the slope characterises all the models, the extrapolation method is valid in a model-independent way.

As explained in section 6.1.3, the extrapolation of the elastic cross-section to $t = 0$ will be based on the measurement of the $d\sigma/dt$ ($d\sigma/dt_y$) distribution for the $\beta^* = 1540\,\text{m}$ ($\beta^* = 90\,\text{m}$) optics. For the $\beta^* = 90\,\text{m}$ optics, the azimuthal symmetry of the elastic scattering process, i.e. the equality of the distributions of t_y and t_x, is used to infer the distribution $\text{d}\sigma/\text{d}t$ from the $\text{d}\sigma/\text{d}t_y$ distribution.

The accuracy of the extrapolation to $t = 0$ is shown in figure 6.7. The key contributions are the following:

- Smearing effects of the t-measurement: For $\beta^* = 90$, they are dominated by the beam divergence ($\sigma(\theta_{\text{beam}}) = 2.3\ \mu$rad) and lead to a shift of -2% in the extrapolation result (figure 6.7 left). For $\beta^* = 1540\,$m with $\sigma(\theta_{\text{beam}}) = 0.29\ \mu$rad, this contribution is less than 0.1% (figure 6.7 right).

- The statistical error of the extrapolation with the $\beta^* = 90\,$m optics for an integrated luminosity of $2\,\text{nb}^{-1}$, i.e. about 5 hours running at a luminosity of $10^{29}\,\text{cm}^{-2}\,\text{s}^{-1}$, ranges between 0.6% and 4% depending on the fit interval for the extrapolation. For the $\beta^* = 1540\,$m optics, this contribution is less than 0.1% for an integrated luminosity of of $0.36\,\text{nb}^{-1}$, i.e. about 10 hours of running at a luminosity of $10^{28}\,\text{cm}^{-2}\,\text{s}^{-1}$.

- Systematic uncertainty of the t-measurement: the dominant contribution comes from the uncertainty of the effective length L_x. The currently expected precision of 2% would translate into an offset of the extrapolation of about 4%. Detector alignment and beam position accuracy are much more crucial for the $\beta^* = 1540\,$m optics with its small beam size (the vertical beam size $\sigma_{y_{\text{beam}}} = 80\,\mu$m at the 220 m RP station) than for $\beta^* = 90\,$m, where $\sigma_{y_{\text{beam}}} = 625\,\mu$m at the 220 m RP station.

- Model-dependent deviations of the nuclear elastic pp cross-section from an exponential shape lead to a bias in the extrapolation. Besides the Islam et al. model [7], which can be excluded or confirmed by the measured t-distribution at large $|t|$-values, the models are within $\pm 1\%$ ($\beta^* = 90\,$m) or $\pm 0.2\%$ ($\beta^* = 1540\,$m).

6.3.3 The ρ parameter

The ρ parameter, estimated to be about 0.14 by extrapolating measurements at lower energies [5], enters σ_{tot} in the factor $1/(1+\rho^2) \sim 0.98$, and hence gives only a relative contribution of about 2%. Assuming a relative uncertainty of at most 33% on ρ, determined by the error of the measurements at TEVATRON [4] and the extrapolation to LHC energies, we expect an relative uncertainty contribution of less than $\delta(1+\rho^2)/(1+\rho^2) = 1.3\%$.

6.3.4 Combined uncertainty on total cross-section and luminosity

Combining all the above uncertainties by error propagation for the expressions

$$\sigma_{\text{tot}} = \frac{16\pi}{1+\rho^2} \cdot \frac{dN_{\text{el}}/dt|_{t=0}}{N_{\text{el}} + N_{\text{inel}}} \quad \text{and} \tag{6.2}$$

$$\mathscr{L} = \frac{1+\rho^2}{16\pi} \cdot \frac{(N_{\text{el}} + N_{\text{inel}})^2}{dN_{\text{el}}/dt|_{t=0}}\,, \tag{6.3}$$

and taking into account the correlations, yields a relative error of 4% on σ_{tot} and a relative uncertainty of 7% on $\mathscr{L}$ with $\beta^* = 90\,$m. With $\beta^* = 1540\,$m the expected precision is at the 1% level but this requires an improved knowledge of the optical functions and an alignment precision of the RP station better than $50\,\mu$m.